Three-Dimensional Nanolithography Using Light Scattering from Colloidal Particles

Xu A. Zhang, Jonathan Elek, and Chih-Hao Chang*

Department of Mechanical and Aerospace Engineering, North Carolina State University, Raleigh, North Carolina 27695, United States

ABSTRACT The interaction between light and colloidal elements can result in a wealth of interesting near-field optical patterns. By examining the optical and colloidal properties, the intensity distribution can be tailored and harnessed for three-dimensional nanolithography. Here, we examine the use of light scattering from colloidal particles to fabricate complex hollow nanostructures. In this approach, a single colloidal sphere is illuminated to create a scattering pattern, which is captured by a photoresist in close proximity. No external optical elements are required, and the colloidal elements alone provide the modulation of the optical intensity pattern. The fabricated nanostructures can be designed to have multiple shells, confined volumes, and single top openings, resembling "nano-volcanoes." The geometry of such structures is dependent on the scattered light distribution and can be accurately modeled by examining the light—particle interaction. The hollow nanostructures can be used to trap nanomaterial, and we demonstrate their ability to trap 50 nm silica nanoparticles. These well-defined surface hollow structures can be further functionalized for applications in controlled drug delivery and biotrapping. Colloidal elements with different geometries and material compositions can also be incorporated to examine other light—colloid interactions.

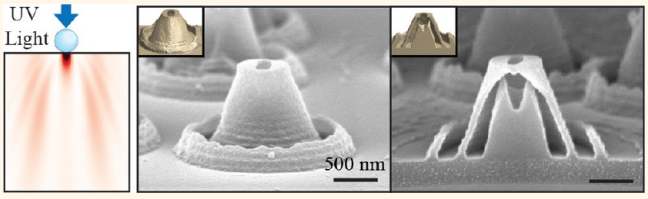

KEYWORDS: nanolithography · three-dimensional nanostructures · colloids · self-assembly · light scattering

Three-dimensional (3D) nanostructures have many inherent advantages, and they have enabled a number of key innovations in nanoscience in recent years. For example, high surface area-to-volume ratio of 3D structures can yield more efficient energy conversion in solar cells[1] and ultrafast battery electrodes.[2] Properly designed periodic 3D nanostructures can be used as photonic[3−5] and phononic[6] crystals. High aspect ratio surface nanostructures can also lead to bioinspired anti-reflection and self-cleaning surfaces.[7,8] In biomedical areas, hollow nanostructures and nanoparticles have been investigated for drug delivery systems due to their unique capability to precisely hold and release drugs.[9−13] Various "top-down" 3D lithography approaches have been used to enable these advances, including layer-by-layer techniques,[3−5] focused ion beam milling,[14] and electron-beam lithography.[15] One particular effective 3D patterning technique that has drawn significant research interest is direct-write two-photon polymerization, which allows patterning of arbitrary structures in 3D space.[16−19] However, since this is inherently a serial process where focused light is scanned across the sample to expose individual voxels, the write time increases significantly for large areas. This technique also requires elaborate system hardware, including ultrafast pulsed lasers, scanning optics, and feedback control electronics. While these techniques are effective in creating complex structures, they can be costly and difficult to scale up for manufacturing. One attractive method for large-area patterning is phase-shift lithography based on the Talbot effect,[20−24] where a two-dimensional (2D) phase mask is illuminated to generate a periodic 3D intensity pattern. This method requires a single exposure, resulting in 3D lithography with high-throughput and scalability. This technique has been demonstrated to be effective when used in conjunction with phase masks fabricated using deep-ultraviolet,[21] interference,[22] Dip-Pen,[23] and electron-beam lithography.[24]

Among the diverse emerging nanofabrication methods, colloidal-based technique has also drawn wide attention.[25−42] These "bottom-up" techniques exploit colloidal

* Address correspondence to chichang@ncsu.edu.

Received for review April 29, 2013 and accepted June 5, 2013.

Published online June 05, 2013
10.1021/nn402637a

particles as elementary building blocks, where the particles self-assemble to form 3D structures[25−29] or act as physical masks for subsequent additive deposition[30−34,37] or subtractive etching.[35−37] These techniques can yield high-quality nanostructures, such as hemispherical metal caps,[34] nanopores,[35] and sculptured colloids[36] with relatively low costs. Recently, we demonstrated that close-packed colloidal arrays can also be used as an optical phase mask to fabricate periodic 3D nanostructures with controllable lattice parameters.[38] By harnessing the optical interaction with colloidal elements, 3D patterning with more design parameters can be enabled by controlling both optical and colloidal parameters.

In this work, we investigate the use of light scattering from individual colloidal elements for 3D nanolithography. In the proposed method, isolated particle focuses and scatters normal-incident light into multiple intensity lobes, which is governed by the scattering characteristics. The intensity pattern can then be recorded by underlying photosensitive materials, resulting in 3D hollow shell-like structures. We focus on the Mie scattering regime for a spherical particle, where the particle diameter D is comparable to wavelength λ. In this regime, the angular-variant scattering profile can result in complex 3D intensity patterns. No masks are needed in this approach, and the colloidal elements are assembled directly on the photoresist. There has been exciting work utilizing near-field light focusing from individual colloidal particles for nanolithography,[43−45] but they have been limited to 2D patterns. This work explores using colloidal light scattering to fabricate 3D geometries. While in this study we focus on dielectric nanospheres, other colloids with nonspherical geometries[35−38] can be incorporated into this technique. Metallic nanoparticles can also be utilized to enable localized plasmonic interactions for subwavelength patterning. The proposed method can also be utilized for 3D visualization of near-field enhancement of plasmonic nanostructures.[46] Particle light scattering is a well-known phenomenon and historically has been used to determine particle size distribution in colloidal solutions[47] and to study aerosols in the atmosphere,[48] but in this work, they are employed for 3D lithography.

The proposed method is illustrated in Figure 1, where a single nanosphere scatters normal-incident UV light into one main and multiple side lobes to form a complex 3D intensity distribution. The scattering field is calculated using finite-difference time-domain (FDTD) method.[49] An underlying photoresist layer is used to record this intensity pattern, as shown in Figure 1b. When a positive-tone photoresist is used, a hollow shell-like 3D "nano-volcano" can be obtained, as illustrated in Figure 1c. These structures are hollow, and the only opening is located on the top side. The slanted shell is defined by the minima of the side lobes, and its angle θ and thickness t can be controlled. The key parameter in this process is the ratio of the particle diameter to the

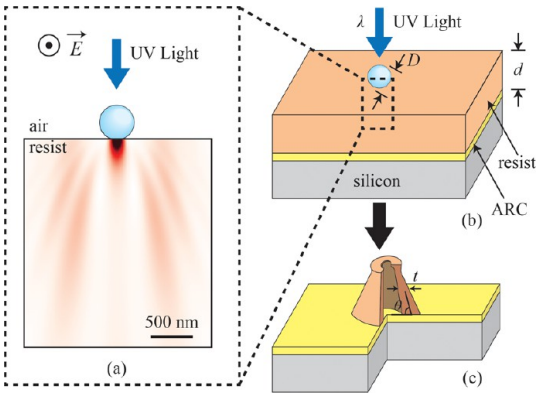

Figure 1. Fabrication process of the hollow 3D nanostructures using light scattering from a colloidal nanoparticle. (a) FDTD simulation showing the scattering intensity pattern produced by TE-polarized UV light and a single nanosphere. Red and white indicate high and low intensities, respectively. (b) Intensity pattern is recorded by an underlying photoresist layer on top of an ARC layer. (c) Diagram showing the resulting 3D hollow nano-volcano structure.

exposure wavelength, $\gamma = D/\lambda$, which determines the scattering regime. The diameter of the particle used here is selected to be comparable to the exposure wavelength so the light scattering would be in the Mie scattering regime ($\gamma \sim 1$), resulting in alternating bright and dark side lobes that define the nanostructure shells. Outside of this regime, the scattered light will either result in uniform angular distribution, as observed in the Rayleigh scattering ($\gamma \ll 1$), or in mostly focusing, as shown in the solution of geometrical optics ($\gamma \gg 1$). By varying and controlling γ in the Mie scattering regime, the patterned 3D nanostructures can be designed.

RESULTS AND DISCUSSION

Scanning electron microscope (SEM) images of the fabricated 3D nanostructures are shown in Figure 2. In these experiments, linearly polarized 325 nm laser was used to illuminate particles with diameters of 450 nm, 750 nm, and 1.9 μm. The micrographs in each row represent the side and cross-section views of the hollow nanostructures patterned with TE- and TM-polarized light, respectively, for the three different diameter spheres. Minor differences between the different polarization exposures can be observed, indicating the patterned nanostructures have a two-fold symmetry. The inset in each micrograph depicts the simulated structure using FDTD method and a binary resist model. Mie theory can also be used to predict the angular intensity profile of the scattered pattern but cannot accurately model the effect of multiple film layers (for details, see Supporting Information A). Every structure has sloped sidewalls with an opening on top and is hollow inside, resembling a nano-volcano. By varying the particle diameter-to-wavelength ratio γ, the structures can be designed with and without an inner core, as shown in Figure 2a−d and Figure 2e−l, respectively. The angle of the sidewall is also dependent on γ

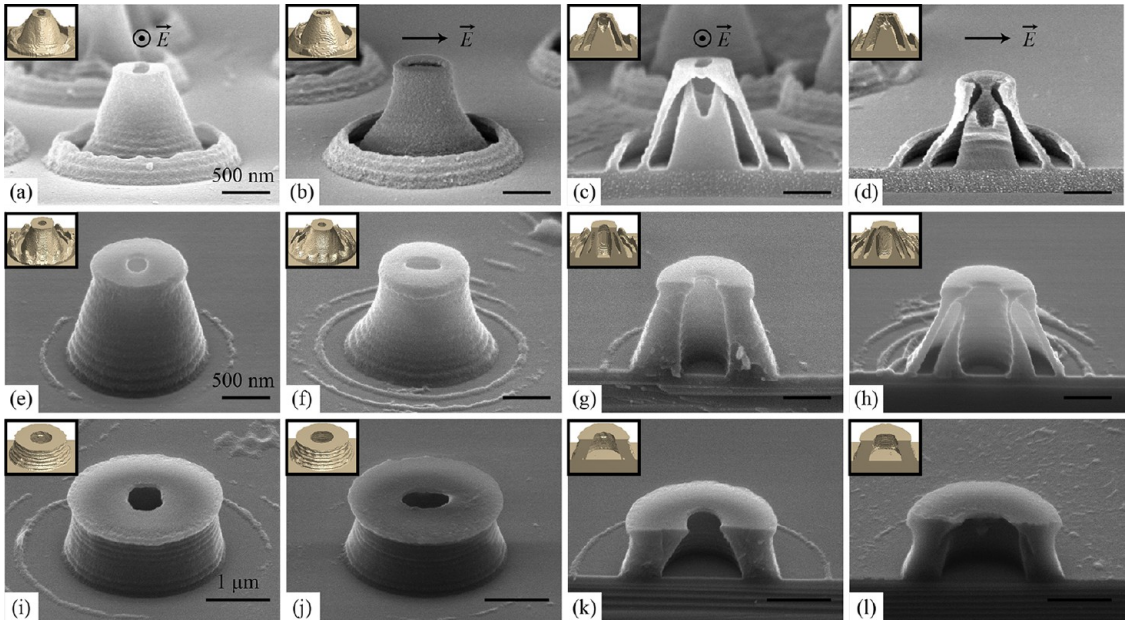

Figure 2. Micrographs of the fabricated hollow 3D nanostructures using TE- and TM-polarized 325 nm illuminations. The inset diagrams show the corresponding simulated nanostructures using FDTD method and a binary resist model. The nanostructures in each row were fabricated under the same conditions: (a–d) particle diameter D = 450 nm, exposure dose = 130 mJ/cm^2, γ = 1.38; (e–h) D = 750 nm, exposure dose = 120 mJ/cm^2, γ = 2.30; (i–l) D = 1.9 1m, exposure dose = 130 mJ/cm^2, γ = 5.85.

and can be designed to be 67 to 83°. The exposure dose is another factor that affects sidewall thickness and the inner core geometry. We have shown that the sidewall thickness can be controlled down to 60 nm.

The colloidal light scattering can be described using the FDTD and binary resist models developed (Supporting Information A), and the nano-volcano dimensions can be accurately predicted. Figure 3 illustrates a quantitative comparison of the patterned and predicted structures using a 1 μm diameter particle and 325 nm wavelength TE-polarized exposure (γ = 3.08). The sidewall angles and thicknesses are compared, showing good agreement between the experiment and simulation. Note that the voids in the sidewall of the simulated cross section are enclosed spaces and cannot be dissolved by the developer in the experiments, forming a thick solid sidewall. These FDTD and binary resist models were used to predict all simulated nano-volcano structures in this work. The relationships of exposure dose with sidewall angle, sidewall thickness, and the top geometry of the nano-volcanoes are described in more detail in Supporting Information B.

Since the lithographic exposure is governed by the light scattering profile in the Mie scattering regime, the fabricated structure can be designed by controlling the particle diameter-to-wavelength ratio γ. To illustrate this dependency, the sidewall angles of the nano-volcanoes are compared with respect to different exposure γ values, as shown in Figure 4. Here the sidewall angle values are experimentally measured using cross-section SEM micrographs and compared with theoretical predictions using FDTD method.

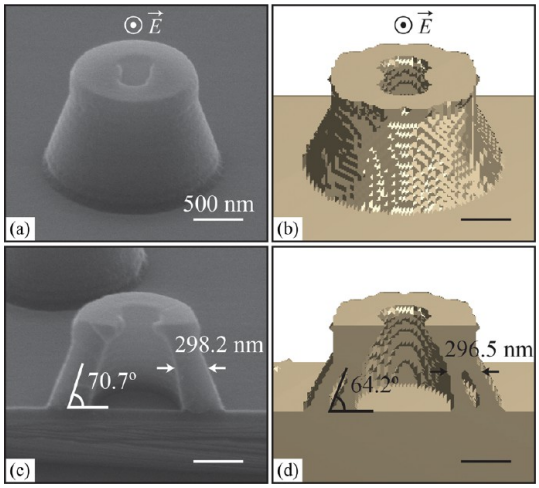

Figure 3. Structure prediction using FDTD and binary resist models for nano-volcano. Diagram (a) and (b) compare the side geometries between the fabricated and simulated structures, respectively, while (c) and (d) present a quantitative comparison of the same fabricated and simulated nano-volcano interiors, respectively.

Based on the values of γ, the geometries of the nano-volcanoes can be divided into three regimes, as represented by the colors. In region I, where $\gamma < 1.3$, the intensity minima of the first side lobes of the colloidal scattering pattern define the outer sidewall, and thus the angle increases as γ increases. The structures in this region are coreless and have nearly vertical sidewalls when γ approaches 1.3, which defines the boundary (black dashed line) between regions I and II. The dashed lines connecting regions I and II represent the transitional region, where $1.2 < \gamma < 1.4$ and the

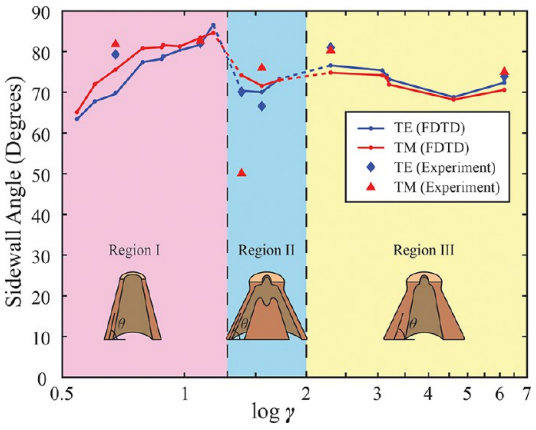

Figure 4. Operating shape diagram of the patterned 3D structures, showing the experimental results and FDTD simulations of the sidewall angle θ with respect to γ. Three regions of the achievable hollow nano-volcano structures are presented in the diagrams. The dashed lines connecting the adjacent regions represent transitional regions, where shell damages are observed. The black dashed lines are representative boundaries between regions, which are given by γ = 1.3 and 2.

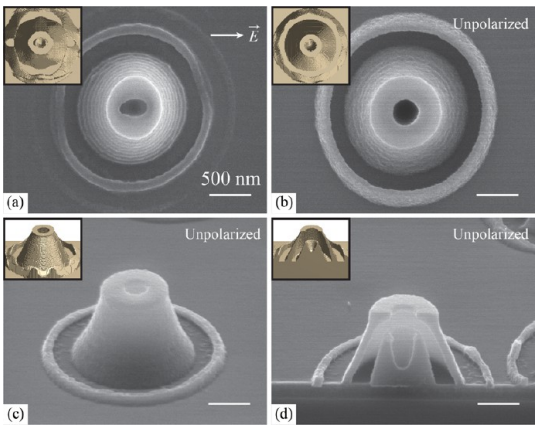

Figure 5. Micrographs showing the polarization effect on the structural symmetry. (a) Top view of a nanostructure fabricated using a linearly polarized 325 nm laser and 500 nm diameter particles with exposure dose of 130 mJ/cm^2 overlaid with the simulated structure. (b–d) Top, side and cross-section views of the nanostructures fabricated using an unpolarized mercury lamp narrow-band filtered at 365 and 500 nm diameter particles. The cylindrical symmetry can be observed.

nano-volcanoes tend to collapse due to thin and porous shells. In region II, the intensity minima of the second side lobes define the outer sidewalls, resulting in lower angles than those defined by the first intensity lobes. The first side lobes still exist at higher scattering angles, resulting in the formation of an inner core within the hollow structure, as shown in the diagram. Because the sidewalls are usually very thin in this region (~60–100 nm), the shell can sometimes sag due to mechanical instability, as indicated in the curved sidewall shown in Figure 2d, when γ = 1.38. Note that the simulated pattern using FDTD for the corresponding exposure condition predicts straight sidewalls. In region III, where $\gamma > 2$, hollow and coreless nano-volcanoes with thick sidewalls can be fabricated. The thick sidewall results from a combination of the first and second side lobes, as the scattering field becomes too close to form separate structures and results in a sidewall with undeveloped volume, as seen in Figure 3. Figure 4 gives a comprehensive summary of the three regions, representing an operating shape diagram to the available nanostructures that can be patterned. Based on specific application, the appropriate geometry can be chosen by designing the corresponding γ value. Note that the shape diagram shown in Figure 4 is unitless, and it can be scaled to fabricate nano-volcanoes of any length scale.

In addition to γ and dose, the polarization state of the incident light can also have an impact on the patterned structures. Since the spherical colloidal elements used in this work are circularly symmetric, the symmetry of the patterned nano-volcanoes is solely dependent on the polarization state of the illumination. The fabrication results using a linearly polarized laser illustrate the two-fold symmetry of the nanostructures, as shown in Figure 2. This symmetry can be better observed in the top-view micrograph for a sample with γ = 1.54, as shown in Figure 5a, where the long axis of the elliptical opening is aligned to the polarization direction. When the exposure light is unpolarized, the fabricated nano-volcanoes have cylindrical symmetry, as shown in Figure 5b–d. These structures were fabricated using 500 nm diameter particles and an unpolarized mercury lamp narrow-band filtered at 365 nm. The value of γ is in region II of Figure 4, and an inner core can be observed in the nano-volcano, agreeing with the previous model. This result supports the conclusion that the phase diagram illustrated in Figure 4 is also applicable to unpolarized illuminations, which is expected given that the simulated TE and TM cases are similar. The shape of the particle can also affect the symmetry of the resultant nanostructures. If nonspherical colloidal elements are used, such as cubic particles or nanorods, the resultant structures are expected to resemble the symmetry of the elements and more complex geometries can be obtained.

The hollow nano-volcano structures can also be patterned in a periodic array using light scattering from hexagonal non-close-packed particles, which allows precise spatial control of the surface structures. In this approach, individual nanoparticles are placed in a periodic array that has a larger period than the particle diameters. This particular type of assembly was achieved *via* isotropic oxygen plasma etching of a monolayer of close-packed micrometer-size polystyrene nanospheres.[50] The plasma etching can preserve the spherical shape and the periodic order of the particles while reducing the particle diameter. Detailed simulations, fabrication process, and characterizations can be found in Supporting Information C. Three types of periodic arrays using

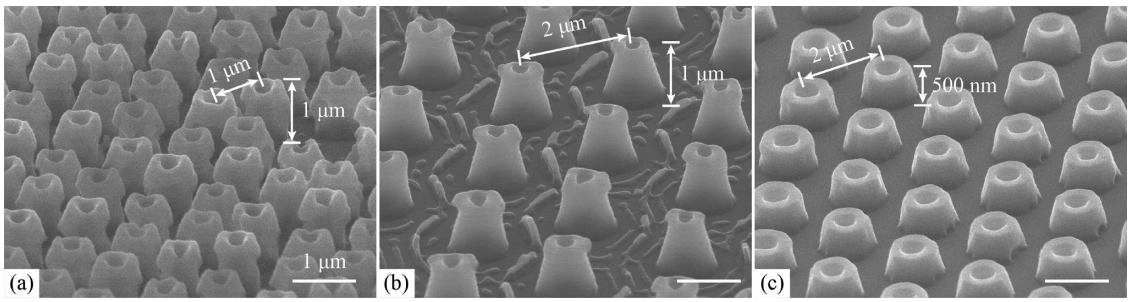

Figure 6. Micrographs of the periodic nano-volcano arrays with (a) 1 μm period and 1 μm height, (b) 2 μm period and 1 μm height, (c) 2 μm period and 500 nm height.

different initial sphere diameters and resist thicknesses were fabricated, as shown in Figure 6. The individual structure in each array has a hollow structure, similar to the isolated ones fabricated in the previous sections. The periods depend on the initial size of the nanospheres prior to size reduction and are 1 and 2 μm, as shown in Figure 6a,b, respectively. Structural defects, such as broken lower sidewalls in Figure 6a, can be observed due to light interference between overlapping scattering fields from neighboring particles. By reducing the thickness of the photoresist to 500 nm, the same 2 μm period array can have improved structural quality, as shown in Figure 6c. The thickness of photoresist should be chosen within the height limit to avoid light interference between neighboring particles, which depends on the particle array period and the particle diameter-to-wavelength ratio. The dependency of these factors on structure control is currently under investigation.

Application in Particle Trapping. The proposed method harnesses colloidal light scattering for facile fabrication of hollow 3D nano-volcano structures, which can find applications in functionalized surfaces for particle/cell trapping and drug delivery. Hollow nanostructures have drawn particular interests in these areas, and researchers have successfully demonstrated well-controlled drug loading and release mechanisms.[9−13] Using the hollow shell-like nanostructures fabricated in this work, we investigate its particle trapping capability using vacuum. In this approach, the nano-volcano sample was covered by a film of aqueous colloidal solution with 50 nm diameter silica nanoparticles (Polyscience colloidal silica microspheres in 5% aqueous solution) and placed in a vacuum chamber. The vacuum degasses the trapped air bubbles inside the nano-volcano structures, allowing the solution to fill the hollow chambers. The samples were allowed to dry in atmosphere, loading the nanoparticles within the nano-volcanoes. The extra particles outside the nanostructures were removed using ultrasonic agitation, while the particles within the chamber remained trapped. The particle trapping capability of the fabricated structure is illustrated in Figure 7a,b, where the interiors of double-shelled and thick-walled nano-volcanoes after particle loading are shown, respectively.

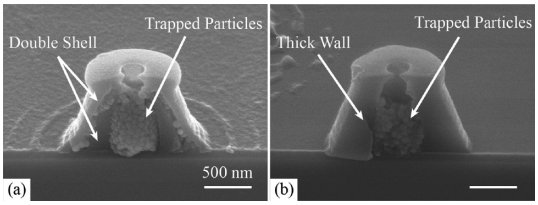

Figure 7. Micrographs of particle-trapping nano-volcanoes. The 50 nm diameter silica particles are trapped in (a) double-shelled and (b) thick-walled nano-volcanoes.

The silica particles can be trapped efficiently within the interior chamber of the nano-volcanoes, while no particles can be observed outside the nano-volcanoes. This trapping mechanism is also uniform, and nano-volcanoes over an area of 5.9 mm^2 were found loaded. Given the nanoscale volume, a finite number of particles were trapped, which can be used for precise drug delivery. In these experiments, the double-shelled nano-volcanoes shown in Figure 7a can collapse under high vacuum because their thin sidewalls (~60 nm) are mechanically unstable. Therefore, thick-walled nano-volcanoes are preferred to withstand high vacuum in this loading mechanism, as indicated in region III of the shape diagram shown in Figure 4. Release and other loading mechanisms with less structural damages are currently being explored. While all structures in this work are pattern in polymer, other materials may be introduced by using conformal deposition techniques such as atomic layer deposition. This will allow structures that are mechanically more stable and enable further surface functionalization of the nano-volcanoes. We will examine the use of periodic nano-volcano arrays to enhance the spatial control of particle trapping or delivery.

CONCLUSION

In this work, we have demonstrated the fabrication of complex 3D hollow nanostructures using light scattering from individual colloidal elements and its application in particle trapping. This approach harnesses the local optical interaction with colloids and allows versatile, facile fabrication of complex 3D nano-volcano structures. No external optics are required in this approach, and light is manipulated into the designed

optical pattern solely by the colloids. The scattering field is well described by the proposed shape diagram, and various geometries can be readily fabricated by controlling the particle size-to-wavelength ratio. The 3D nanostructures can also be patterned with periodic order using non-close-packed colloidal assembly, allowing precise spatial control for particle trapping/delivery. The nanoscale interior volume of the hollow nano-volcano structures has been shown to be effective in trapping nanoparticles and can potentially be used as functionalized patches for particle/cell trapping and precise drug delivery. Other possible applications involve biosensing and optical or acoustic focusing using the tapered sidewalls. Although in this work we focused on readily available spherical nanoparticles as scattering objects, other types of colloidal elements, such as cubic, tetrahedral, and rod particles, can be incorporated into this approach to enable a wide variety of achievable 3D nanostructures.

METHODS

Sample Preparation. In all experiments, the samples were prepared on silicon substrates. A layer of anti-reflection coating (ARC i-CON-16, Brewer Science, Inc.) was used to reduce back reflection. The anti-reflection coating is designed to reduce back reflection from the resist and ARC interface, and its thickness is optimized to minimize normal-incident light. The ARC thickness is around 90 and 160 nm for the 325 and 365 nm wavelength exposures, respectively. Positive photoresist (Sumitomo PFi88A7) was spin-coated on the ARC layer. The thickness of the photoresist layer should be thick enough to capture the scattering pattern and depends on the choice of particle size. However, the thickness is limited by the absorption of the photoresist material, as light intensity decays exponentially into the material. A range of 0.5 to 1.5 μm thickness was used for the particle size range used in our experiments. To enhance sphere adhesion and facilitate the spreading of the aqueous colloidal solution, a 10 nm thick layer of silicon dioxide was deposited on top of the resist surface using electron-beam evaporation. It is designed to be thin enough to have minimal optical effects on the scattering pattern. Monodispersed polystyrene spheres with various diameters from 350 nm to 1.9 μm (Polyscience Polybead Microspheres in 2.5% aqueous solution) were used as scattering objects in the experiments. The solution was spin-coated on the prepared sample to assemble isolated nanospheres.

Lithographic exposures were performed using either a linearly polarized 325 nm He−Cd laser or an unpolarized mercury lamp narrow-band filtered at 365 nm. After exposing the samples with doses of 100−200 mJ/cm^2, the nanospheres were removed by ultrasonic agitation and the thin silicon dioxide layer was etched using buffered HF (J.T. Baker, buffered oxide etch 10:1). The exposed samples were then developed in 2.4% tetramethylammonium hydroxide (TMAH) developer solution (Microposit MF-CD-26) for 1−2 min. The samples were characterized using top view and cross-section view scanning electron microscope (JEOL 6400F) at 5 keV.

Simulation and Modeling. The colloidal light scattering intensity distribution in the photoresist was modeled using finite-difference time-domain (FDTD) methods. The results were also compared with the results from the analytical Mie scattering solutions, as described in Supporting Information A. A binary photoresist model was used to predict the resulting structures, where any volume above a threshold dose was completely removed. The intensity profile through the thickness of the resist was assumed to have an exponential decay to model the resist absorption. The geometries of the simulated structures are then quantitatively analyzed in Matlab. The predicted models are depicted as inset diagrams with their corresponding fabrication results.

Conflict of Interest: The authors declare no competing financial interest.

Acknowledgment. We gratefully acknowledge the students, staff, and facility support from the North Carolina State University Nanofabrication Facility (NNF). This work was supported by a NASA Office of the Chief Technologist's Space Technology Research Opportunity−Early Career Faculty grant (Grant NNX12AQ46G) and by the National Science Foundation (Grant EEC-1160483) through the Nanosystems Engineering Research Center for Advanced Self-Powered Systems of Integrated Sensors and Technologies (ASSIST).

Supporting Information Available: Additional information on theoretical structure prediction, exposure dose dependency of nano-volcano geometry, and fabrication of periodic nano-volcano arrays. This material is available free of charge *via* the Internet at http://pubs.acs.org.

REFERENCES AND NOTES

1. Fan, Z.; Razavi, H.; Do, J.; Moriwaki, A.; Ergen, O.; Chueh, Y.-L.; Leu, P. W.; Ho, J. C.; Takahashi, T.; Reichertz, L. A.; *et al.* Three-Dimensional Nanopillar-Array Photovoltaics on Low-Cost and Flexible Substrates. *Nat. Mater.* **2009**, *8*, 648–653.
2. Zhang, H.; Yu, X.; Braun, P. V. Three-Dimensional Bicontinuous Ultrafast-Charge and -Discharge Bulk Battery Electrodes. *Nat. Nanotechnol.* **2011**, *6*, 277–281.
3. Lin, S. Y.; Fleming, J. G.; Hetherington, D. L.; Smith, B. K.; Biswas, R.; Ho, K. M.; Sigalas, M. M.; Zubrzycki, W.; Kurtz, S. R.; Bur, J. A Three-Dimensional Photonic Crystal Operating at Infrared Wavelengths. *Nature* **1998**, *394*, 251–253.
4. Noda, S.; Tomoda, K.; Yamamoto, N.; Chutinan, A. Full Three-Dimensional Photonic Bandgap Crystals at Near-Infrared Wavelengths. *Science* **2000**, *289*, 604–606.
5. Qi, M.; Lidorikis, E.; Rakich, P. T.; Johnson, S. G.; Joannopoulos, J. D.; Ippen, E. P.; Smith, H. I. A Three-Dimensional Optical Photonic Crystal with Designed Point Defects. *Nature* **2004**, *429*, 538–542.
6. Jang, J.-H.; Ullal, C. K.; Gorishnyy, T.; Tsukruk, V. V.; Thomas, E. L. Mechanically Tunable Three-Dimensional Elastomeric Network/Air Structures *via* Interference Lithography. *Nano Lett.* **2006**, *6*, 740–743.
7. Min, W.-L.; Jiang, B.; Jiang, P. Bioinspired Self-Cleaning Antireflection Coatings. *Adv. Mater.* **2008**, *20*, 3914–3918.
8. Park, K.-C.; Choi, H. J.; Chang, C.-H.; Cohen, R. E.; McKinley, G. H.; Barbastathis, G. Nanotextured Silica Surfaces with Robust Superhydrophobicity and Omnidirectional Broadband Supertransmissivity. *ACS Nano* **2012**, *6*, 3789–3799.
9. Li, Z.-Z.; Wen, L.-X.; Shao, L.; Chen, J.-F. Fabrication of Porous Hollow Silica Nanoparticles and Their Applications in Drug Release Control. *J. Controlled Release* **2004**, *98*, 245–254.
10. Lou, X. W.; Archer, L. A.; Yang, Z. Hollow Micro-/Nanostructures: Synthesis and Applications. *Adv. Mater.* **2008**, *20*, 3987–4019.
11. Yavuz, M. S.; Cheng, Y.; Chen, J.; Cobley, C. M.; Zhang, Q.; Rycenga, M.; Xie, J.; Kim, C.; Song, K. H.; Schwartz, A. G.; *et al.* Gold Nanocages Covered by Smart Polymers for Controlled Release with Near-Infrared Light. *Nat. Mater.* **2009**, *8*, 935–939.
12. Moon, G. D.; Choi, S.-W.; Cai, X.; Li, W.; Cho, E. C.; Jeong, U.; Wang, L. V.; Xia, Y. A New Theranostic System Based on Gold Nanocages and Phase-Change Materials with Unique Features for Photoacoustic Imaging and Controlled Release. *J. Am. Chem. Soc.* **2011**, *133*, 4762–4765.
13. Tao, S. L.; Desai, T. A. Microfabricated Drug Delivery Systems: From Particles to Pores. *Adv. Drug Delivery Rev.* **2003**, *55*, 315–328.

14. Jeon, J.; Floresca, H. C.; Kim, M. J. Fabrication of Complex Three-Dimensional Nanostructures Using Focused Ion Beam and Nanomanipulation. *J. Vac. Sci. Technol., B* **2010**, *28*, 549–553.
15. Yamazaki, K.; Yamaguchi, H. Three-Dimensional Alignment with 10 nm Order Accuracy in Electron-Beam Lithography on Rotated Sample for Three-Dimensional Nanofabrication. *J. Vac. Sci. Technol., B* **2008**, *26*, 2529–2533.
16. Maruo, S.; Nakamura, O.; Kawata, S. Three-Dimensional Microfabrication with Two-Photon-Absorbed Photopolymerization. *Opt. Lett.* **1997**, *22*, 132–134.
17. Cumpston, B. H.; Ananthavel, S. P.; Barlow, S.; Dyer, D. L.; Ehrlich, J. E.; Erskine, L. L.; Heikal, A. A.; Kuebler, S. M.; Lee, I.-Y. S.; McCord-Maughon, D.; *et al.* Two-Photon Polymerization Initiators for Three-Dimensional Optical Data Storage and Microfabrication. *Nature* **1999**, *398*, 51–54.
18. Kawata, S.; Sun, H.-B.; Tanaka, T.; Takada, K. Finer Features for Functional Microdevices. *Nature* **2001**, *412*, 697–698.
19. Haske, W.; Chen, V. W.; Hales, J. M.; Dong, W.; Barlow, S.; Marder, S. R.; Perry, J. W. 65 nm Feature Sizes Using Visible Wavelength 3-D Multiphoton Lithography. *Opt. Express* **2007**, *15*, 3426–3436.
20. Shir, D.; Nelson, E. C.; Chen, Y. C.; Brzezinski, A.; Liao, H.; Braun, P. V.; Wiltzius, P.; Bogart, K. H. A.; Rogers, J. A. Three Dimensional Silicon Photonic Crystals Fabricated by Two Photon Phase Mask Lithography. *Appl. Phys. Lett.* **2009**, *94*, 011101-1–011101-3.
21. Jeon, S.; Park, J.-U.; Cirelli, R.; Yang, S.; Heitzman, C. E.; Braun, P. V.; Kenis, P. J. A.; Rogers, J. A. Fabricating Complex Three-Dimensional Nanostructures with High-Resolution Conformable Phase Masks. *Proc. Natl. Acad. Sci. U.S.A.* **2004**, *101*, 12428–12433.
22. Jang, J.-H.; Ullal, C. K.; Maldovan, M.; Gorishnyy, T.; Kooi, S.; Koh, C.; Thomas, E. L. 3D Micro- and Nanostructures *via* Interference Lithography. *Adv. Funct. Mater.* **2007**, *17*, 3027–3041.
23. Jang, J.-W.; Zheng, Z.; Lee, O.-S.; Shim, W.; Zheng, G.; Schatz, G. C.; Mirkin, C. A. Arrays of Nanoscale Lenses for Subwavelength Optical Lithography. *Nano Lett.* **2010**, *10*, 4399–4404.
24. Isoyan, A.; Jiang, F.; Cheng, Y. C.; Cerrina, F.; Wachulak, P.; Urbanski, L.; Rocca, J.; Menoni, C.; Marconi, M. Talbot Lithography: Self-Imaging of Complex Structures. *J. Vac. Sci. Technol., B* **2009**, *27*, 2931–2937.
25. Blaaderen, A.; van Ruel, R.; Wiltzius, P. Template-Directed Colloidal Crystallization. *Nature* **1997**, *385*, 321–324.
26. Gates, B.; Qin, D.; Xia, Y. Assembly of Nanoparticles into Opaline Structures over Large Areas. *Adv. Mater.* **1999**, *11*, 466–469.
27. Rycenga, M.; Camargo, P. H. C.; Xia, Y. Template-Assisted Self-Assembly: A Versatile Approach to Complex Micro- and Nanostructures. *Soft Matter* **2009**, *5*, 1129–1136.
28. Xia, Y.; Gates, B.; Yin, Y.; Lu, Y. Monodispersed Colloidal Spheres: Old Materials with New Applications. *Adv. Mater.* **2000**, *12*, 693–713.
29. Dinsmore, A. D.; Hsu, M. F.; Nikolaides, M. G.; Marquez, M.; Bausch, A. R.; Weitz, D. A. Colloidosomes: Selectively Permeable Capsules Composed of Colloidal Particles. *Science* **2002**, *298*, 1006–1009.
30. Hulteen, J. C.; Van Duyne, R. P. Nanosphere Lithography: A Materials General Fabrication Process for Periodic Particle Array Surfaces. *J. Vac. Sci. Technol., A* **1995**, *13*, 1553–1558.
31. Haginoya, C.; Ishibashi, M. Nanostructure Array Fabrication with a Size-Controllable Natural Lithography. *Appl. Phys. Lett.* **1997**, *71*, 2934.
32. Rybczynski, J.; Ebels, U.; Giersig, M. Large-Scale, 2D Arrays of Magnetic Nanoparticles. *Colloids Surf., A* **2003**, *219*, 1–6.
33. Velev, O. D.; Tessier, P. M.; Lenhoff, A. M.; Kaler, E. W. Materials: A Class of Porous Metallic Nanostructures. *Nature* **1999**, *401*, 548–548.
34. Love, J. C.; Gates, B. D.; Wolfe, D. B.; Paul, K. E.; Whitesides, G. M. Fabrication and Wetting Properties of Metallic Half-Shells with Submicron Diameters. *Nano Lett.* **2002**, *2*, 891–894.
35. Moon, J. H.; Kim, W. S.; Ha, J.-W.; Jang, S. G.; Yang, S.-M.; Park, J.-K. Colloidal Lithography with Crosslinkable Particles: Fabrication of Hierarchical Nanopore Arrays. *Chem. Commun.* **2005**, 4107–4109.
36. Choi, D.-G.; Jang, S. G.; Kim, S.; Lee, E.; Han, C.-S.; Yang, S.-M. Multifaceted and Nanobored Particle Arrays Sculpted Using Colloidal Lithography. *Adv. Funct. Mater.* **2006**, *16*, 33–40.
37. Yang, S.-M.; Jang, S. G.; Choi, D.-G.; Kim, S.; Yu, H. K. Nanomachining by Colloidal Lithography. *Small* **2006**, *2*, 458–475.
38. Chang, C.-H.; Tian, L.; Hesse, W. R.; Gao, H.; Choi, H. J.; Kim, J.-G.; Siddiqui, M.; Barbastathis, G. From Two-Dimensional Colloidal Self-Assembly to Three-Dimensional Nanolithography. *Nano Lett.* **2011**, *11*, 2533–2537.
39. Sun, Y.; Xia, Y. Shape-Controlled Synthesis of Gold and Silver Nanoparticles. *Science* **2002**, *298*, 2176–2179.
40. Xia, Y.; Xiong, Y.; Lim, B.; Skrabalak, S. E. Shape-Controlled Synthesis of Metal Nanocrystals: Simple Chemistry Meets Complex Physics? *Angew. Chem., Int. Ed.* **2009**, *48*, 60–103.
41. Henzie, J.; Grünwald, M.; Widmer-Cooper, A.; Geissler, P. L.; Yang, P. Self-Assembly of Uniform Polyhedral Silver Nanocrystals into Densest Packings and Exotic Superlattices. *Nat. Mater.* **2012**, *11*, 131–137.
42. Biacchi, A. J.; Schaak, R. E. The Solvent Matters: Kinetic *versus* Thermodynamic Shape Control in the Polyol Synthesis of Rhodium Nanoparticles. *ACS Nano* **2011**, *5*, 8089–8099.
43. Devilez, A.; Bonod, N.; Wenger, J.; Gérard, D.; Stout, B.; Rigneault, H.; Popov, E. Three-Dimensional Subwavelength Confinement of Light with Dielectric Microspheres. *Opt. Express* **2009**, *17*, 2089–2094.
44. Kühler, P.; García de Abajo, F. J.; Solis, J.; Mosbacher, M.; Leiderer, P.; Afonso, C. N.; Siegel, J. Imprinting the Optical Near Field of Microstructures with Nanometer Resolution. *Small* **2009**, *5*, 1825–1829.
45. Mcleod, E.; Arnold, C. B. Subwavelength Direct-Write Nanopatterning Using Optically Trapped Microspheres. *Nat. Nanotechnol.* **2008**, *3*, 413–417.
46. Geldhauser, T.; Kolloch, A.; Murazawa, N.; Ueno, K.; Boneberg, J.; Leiderer, P.; Scheer, E.; Misawa, H. Quantitative Measurement of the Near-Field Enhancement of Nanostructures by Two-Photon Polymerization. *Langmuir* **2012**, *28*, 9041–9046.
47. McConnell, M. L. Particle Size Determination by Quasielastic Light Scattering. *Anal. Chem.* **1981**, *53*, 1007A–1018A.
48. Menzies, R. T.; Kavaya, M. J.; Flamant, P. H.; Haner, D. A. Atmospheric Aerosol Backscatter Measurements Using a Tunable Coherent CO_2 Lidar. *Appl. Opt.* **1984**, *23*, 2510–2517.
49. Oskooi, A. F.; Roundy, D.; Ibanescu, M.; Bermel, P.; Joannopoulos, J. D.; Johnson, S. G. Meep: A Flexible Free-Software Package for Electromagnetic Simulations by the FDTD Method. *Comput. Phys. Commun.* **2010**, *181*, 687–702.
50. Plettl, A.; Enderle, F.; Saitner, M.; Manzke, A.; Pfahler, C.; Wiedemann, S.; Ziemann, P. Non-Close-Packed Crystals from Self-Assembled Polystyrene Spheres by Isotropic Plasma Etching: Adding Flexibility to Colloid Lithography. *Adv. Funct. Mater.* **2009**, *19*, 3279–3284.